

Kinetic parameter estimation from SPECT cone-beam projection measurements

Ronald H Huesman[†], Bryan W Reutter[†], G Larry Zeng[‡] and Grant T Gullberg[‡]

[†] Center for Functional Imaging, Lawrence Berkeley National Laboratory, University of California, Berkeley, CA 94720, USA

[‡] Department of Radiology, University of Utah, Salt Lake City, UT 84132, USA

Received 31 July 1997

Abstract. Kinetic parameters are commonly estimated from dynamically acquired nuclear medicine data by first reconstructing a dynamic sequence of images and subsequently fitting the parameters to time–activity curves generated from regions of interest overlaid upon the image sequence. Biased estimates can result from images reconstructed using inconsistent projections of a time-varying distribution of radiopharmaceutical acquired by a rotating SPECT system. If the SPECT data are acquired using cone-beam collimators wherein the gantry rotates so that the focal point of the collimators always remains in a plane, additional biases can arise from images reconstructed using insufficient, as well as truncated, projection samples. To overcome these problems we have investigated the estimation of kinetic parameters directly from SPECT cone-beam projection data by modelling the data acquisition process. To accomplish this it was necessary to parametrize the spatial and temporal distribution of the radiopharmaceutical within the SPECT field of view.

In a simulated chest image volume, kinetic parameters were estimated for simple one-compartment models for four myocardial regions of interest. Myocardial uptake and washout parameters estimated by conventional analysis of noiseless simulated cone-beam data had biases ranging between 3–26% and 0–28%, respectively. Parameters estimated directly from the noiseless projection data were unbiased as expected, since the model used for fitting was faithful to the simulation. Statistical uncertainties of parameter estimates for 10 000 000 events ranged between 0.2–9% for the uptake parameters and between 0.3–6% for the washout parameters.

1. Introduction

Kinetic parameters are commonly estimated from dynamically acquired nuclear medicine data by first reconstructing a dynamic sequence of images and subsequently fitting the parameters to time–activity curves generated from regions of interest overlaid upon the reconstructed image sequence. Since SPECT data acquisition involves movement of the detectors (figure 1) and the distribution of radiopharmaceutical changes during the acquisition (figure 2) the data acquired over a revolution of the camera will not generally correspond to any distribution of radionuclide. Projections at different angles come from different distributions, and we refer to such data as being inconsistent. The image reconstruction step can produce erroneous results that lead to biases in the estimated kinetic parameters. If the SPECT data are acquired using cone-beam collimators wherein the gantry rotates so that the focal point of the collimators always remains in a plane, the additional problem of reconstructing dynamic images from insufficient projection samples arises. The

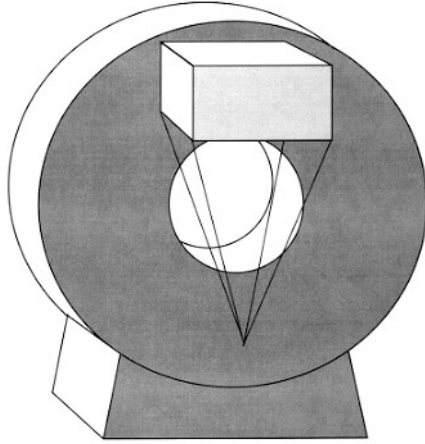


Figure 1. Cone-beam SPECT scanner. The detector rotates about the patient (not shown) so that the focal point remains in a plane perpendicular to the long axis of the patient's body.

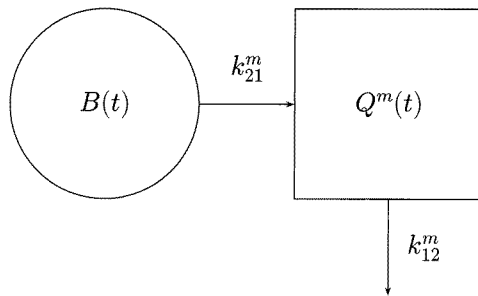


Figure 2. Compartmental model for ^{99m}Tc -teboroxime in the myocardium. $B(t)$ is the blood input function, $Q^m(t)$ is the tracer in tissue type m and k_{21}^m , k_{12}^m are the rate constants for uptake and washout, respectively.

reconstructed intensities will also have errors due to truncated cone-beam projection data, thus producing additional biases in the estimated kinetic parameters.

To overcome these problems we have investigated the estimation of the kinetic parameters directly from the projection data by modelling the data acquisition process of a time-varying distribution of radiopharmaceutical detected by a rotating SPECT system with cone-beam collimation. To accomplish this it was necessary to parametrize the spatial and temporal distribution of the radiopharmaceutical within the SPECT cone-beam field of view. We hypothesize that by estimating directly from cone-beam projections instead of from reconstructed time-activity curves, the parameters which describe the time-varying distribution of radiopharmaceutical can be estimated without bias.

The direct estimation of kinetic parameters from the projection measurements has become an active area of research. However, to our knowledge no one has accomplished direct estimation from full 3D projection data sets. At the University of Michigan, Chiao *et al* (1994a, b) performed estimates of ROI kinetic parameters for a one-compartment model and estimates of parameters of the boundaries for the ROIs from simulated transaxial PET measurements. They demonstrated that the biases in the kinetic parameter estimators were reduced by allowing for estimators of the boundaries of the ROIs to be included in the

estimation process. At Simon Fraser University, Limber *et al* (1995) fitted the parameters of a single exponential decay (to model fatty acid metabolism in the heart) directly from simulated projections acquired with a single rotating SPECT detector system.

Estimation of time–activity curves from projections has been investigated by several groups. We have described a method to estimate the average activity in a 2D region of interest (Huesman 1984), and Defrise *et al* (1990) extended these ideas to 3D. To compensate for physical factors such as attenuation and detector resolution, Carson (1986) described a method to estimate activity density assumed to be uniform in a set of regions of interest using maximum likelihood, and Formiconi (1993) similarly used least squares.

The present research builds on the work of Carson and Formiconi as well as on our previous research (Zeng *et al* 1995) wherein a one-compartment model was fitted to dynamic sequences in a 3×3 array directly from projection measurements. This work showed a bias in estimates from the reconstructed time–activity curves, which was eliminated when estimating the parameters directly from the projections. The estimation was performed in a two-step process: by first estimating the exponential factors using linear time-invariant system theory, then estimating the multiplicative factors using a linear estimation technique. Later we presented preliminary work in 2D (Huesman *et al* 1997) which was the precursor to this 3D research.

The research presented here formulates the problem as a minimization of one nonlinear estimation problem for a 3D time-varying distribution measured with planar orbit cone-beam tomography. A one-compartment model is assumed for the simulated myocardial tissue with a known blood input function, which would correspond to the kinetics of teboroxime in the heart (Smith *et al* 1994, 1996). Parameters are estimated by minimizing a weighted sum of squared differences between the projection data and the model predicted values for a rotating detector SPECT system with cone-beam collimators. The estimation of parameters directly from projections is compared with estimation of kinetic parameters from tomographic determination of time–activity curves for four regions of interest.

2. Estimation of kinetic parameters directly from projections

The parameters are determined from a model of the projection data that assumes a one-compartment kinetic model for each tissue type as shown in figure 2. The expression for uptake in tissue type m is

$$Q^m(t) = k_{21}^m \int_0^t B(\tau) e^{-k_{12}^m(t-\tau)} d\tau = k_{21}^m V^m(t) \quad (1)$$

where $B(t)$ is the known blood input function, k_{21}^m is the uptake parameter, and k_{12}^m is the washout parameter. Total activity in the tissue is given by

$$Q^m(t) + f_v^m B(t) = k_{21}^m V^m(t) + f_v^m B(t) \quad (2)$$

where f_v^m is the fraction of vasculature in the tissue.

This analysis starts with an image volume segmented into blood pool, M tissue types of interest and background as is schematically shown in figure 3. In order to obtain tissue boundaries, the object (patient) is assumed motionless during data acquisition, and the reconstructed image volume (for example, via the projections at the time of strongest signal, or via the summed projections) is segmented to provide anatomical structure. The image intensity at each segmented region is not used. From the segmented image volume the lengths of the blood pool, tissue and background regions along each projection ray for each projection angle are calculated. The number of projection rays per projection angle

is denoted by N , the number of projection angles per rotation by J and the number of rotations by I . Thus, there are a total of $I J N$ projection rays distributed in time and space. For a typical projection ray at angle j and position n , the length of the blood pool along the projection ray is denoted by u_{jn} , the length of the background by v_{jn} and the length of heart tissue m by w_{jn}^m (figure 4). The amplitude of the background activity is denoted by g , and the background is assumed to be proportional to the blood activity. The projection equations can be expressed as

$$p_{ijn} = \int_{t_{ij}-\Delta t}^{t_{ij}} \left\{ u_{jn} B(\tau) + v_{jn} g B(\tau) + \sum_{m=1}^M w_{jn}^m [k_{21}^m V^m(\tau) + f_v^m B(\tau)] \right\} d\tau \quad (3)$$

where the time t_{ij} is equal to $[j + (i - 1)J]\Delta t$. The constants u_{jn} , v_{jn} and w_{jn}^m are pure geometrical weighting factors for blood, background and tissue m , respectively, and these equations are linear in the unknowns g , k_{21}^m and f_v^m . The nonlinear parameters, k_{12}^m , are contained in $V^m(t)$.

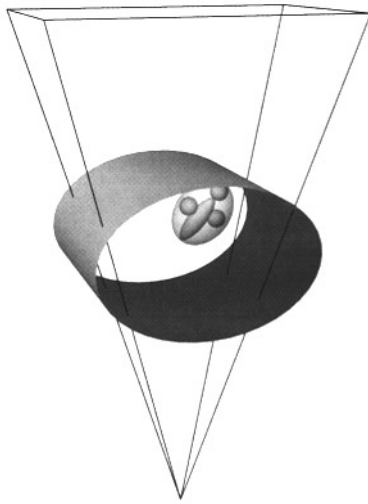


Figure 3. Phantom. The outer surface is the limit of the background activity, and the ellipsoid enclosing the small ellipsoid and three spheres represents the outer surface of the left ventricle. The small ellipsoid is the inner wall of the left ventricle and contains the blood pool.

The criterion which is minimized by varying the model parameters is the weighted sum of squares function

$$\chi^2 = \sum_{i=1}^I \sum_{j=1}^J \sum_{n=1}^N \frac{(p_{ijn} - p_{ijn}^*)^2}{\sigma_{ijn}^2} \quad (4)$$

where p_{ijn}^* are the measured data and σ_{ijn} are their statistical uncertainties. An estimate of the covariance matrix for the resulting model parameters $\hat{\Theta} = (\hat{k}_{12}^m \hat{g} \hat{k}_{21}^m \hat{f}_v^m)$ is

$$\text{cov}(\hat{\Theta}) = \left(\frac{1}{2} \frac{\partial^2 \chi^2}{\partial \Theta^2} \Big|_{\Theta=\hat{\Theta}} \right)^{-1}. \quad (5)$$

Then the statistical uncertainties of the parameter estimates, $\hat{\Theta}$, are the square roots of the diagonal elements of the covariance matrix given by equation (5).

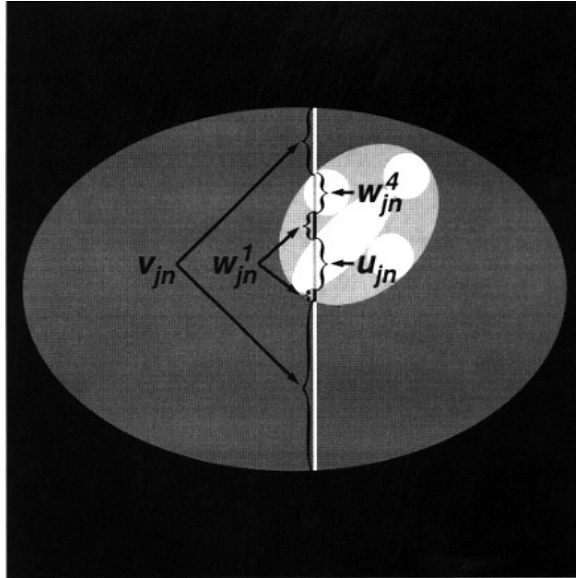


Figure 4. Illustration of lengths along a projection ray for background, v_{jn} , blood pool, u_{jn} , main myocardium, w_{jn}^1 , and septal ROI, w_{jn}^4 .

As mentioned above, equation (3) is a linear function of the parameters g , k_{21}^m , and f_v^m . Therefore the model it describes is called a conditionally linear, partially linear or separable nonlinear model (Bates and Watts 1988, Seber and Wild 1989). Using standard techniques for removing conditionally linear parameters, equation (4) can be considered to be a function of only the nonlinear parameters, k_{12}^m . We have used this technique to obtain the results presented here.

3. Computer simulations

A simulation was performed to evaluate the ability to estimate the kinetic parameters directly from cone-beam projection data. A simulated image volume, shown in figure 3, contained background, blood and four tissue regions of interest. The blood input function and simulated tissue activity curves are shown in figure 5. The blood input function was assumed known, and simple one-compartment models were used within four regions of interest of a simulated left ventricle of the myocardium. Boundaries of the myocardial regions were assumed known, and background activity was proportional to the input function. The parameter g was the ratio of background to blood. There were 13 parameters to estimate: the amplitudes, decay rates and vascular fractions for the four myocardial regions, and the amplitude of the overall background.

The 15 minute data acquisition protocol consisted of ten revolutions of a single-head SPECT system with a detector radius of 30 cm, acquiring 120 angles per revolution and 48 transverse \times 30 axial samples per angle. Attenuation, scatter and geometric point response were not modelled. Each projection had 8.33 mm bin width at the detector, and line length weighting was assumed. The cone-beam collimators had a focal length of 70 cm and yielded a 4.76 mm projection ray spacing at the centre of the tomograph. We also simulated the use of parallel-beam collimators.

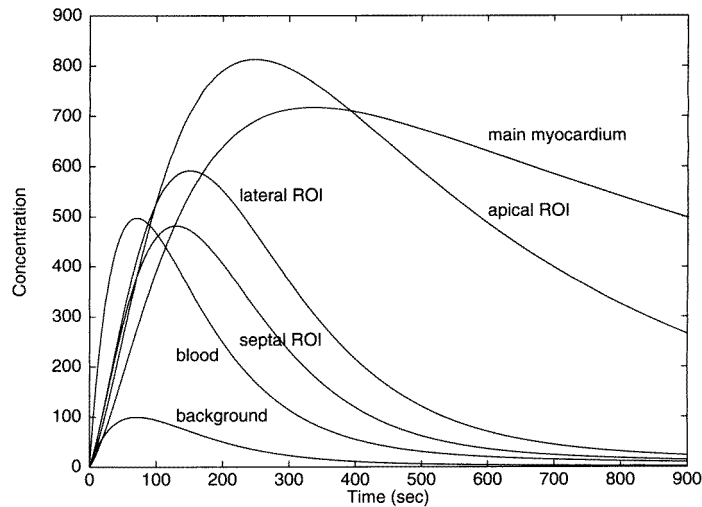


Figure 5. Time-activity curves for blood, background and four tissue regions of interest as shown in figure 3.

For each collimator geometry, a dynamic image sequence was reconstructed and conventional kinetic analysis was performed on time-activity curves obtained by overlaying ROIs upon the reconstructed images. The cone-beam projections were reconstructed into a $48 \times 48 \times 30$ array of $4.76 \text{ mm} \times 4.76 \text{ mm} \times 4.76 \text{ mm}$ volume elements (voxels) using the Feldkamp algorithm (Feldkamp *et al* 1984) and the parallel-beam projections were reconstructed into a $48 \times 48 \times 30$ array of $8.33 \text{ mm} \times 8.33 \text{ mm} \times 8.33 \text{ mm}$ voxels using filtered back-projection. ROIs were defined by taking all voxels containing at least 80% blood pool, background or one of the four tissue types, to ensure that the centres of the voxels were well within the surfaces bounding the anatomical structures of interest. Parameter estimates obtained from conventional analysis of time-activity curves generated from the reconstructed projections were compared with parameters obtained by estimating the time-activity curves from the projections (i.e. the work of Formiconi (1993)). Comparisons were also made with parameters estimated directly from the projections. The results for noiseless projections are shown in tables 1 and 2 and figures 6 and 7.

Parameter estimates obtained from conventional analysis of noiseless, inconsistent, cone-beam projections had biases ranging between 3–26% for the uptake parameters and 0–28% for the washout parameters. The biases were largest for the lateral and septal ROIs, which encompassed small volumes and had relatively fast washout. The estimates obtained using Formiconi's method had smaller biases, ranging between 0.4–17% for the uptake parameters and 0–5% for the washout parameters. Parameters estimated directly from the noiseless projections were unbiased as expected, since the model used for fitting was faithful to the simulation. In addition, multiple local minima were not encountered regardless of noise levels simulated. Estimated parameter uncertainties (see equation (5)) for 10 000 000 total events ranged between 0.2–9% for the uptake parameters and 0.3–6% for the washout parameters.

Parameter estimates were also obtained from noiseless cone-beam projections forced to be consistent over the 90 s time frame of the dynamic data acquisition. Over the course of each revolution of the SPECT system, the activity in each region was held constant at

Table 1. Results of kinetic parameter estimation from noiseless, inconsistent, cone-beam projections: (a) simulated values; (b) values from dynamic reconstructions; (c) values from direct estimation of region time–activity curves (Formiconi 1993); (d) values from direct estimation from projections; (e) uncertainties of values from direct estimation from projections for 10 000 000 events using equation (5). Results of kinetic parameter estimation from noiseless, forced consistent, cone-beam projections: (b') values from dynamic reconstructions; (c') values from direct estimation of region time–activity curves. The units for k_{21}^m and k_{12}^m are min^{-1} .

		a	b	c	d	e	b'	c'
Main myocardium	k_{21}^1	0.540	0.518	0.542	0.540	0.001	0.518	0.540
	k_{12}^1	0.060	0.060	0.060	0.060	0.0002	0.060	0.060
	f_v^1	0.100	0.135	0.102	0.100	0.002	0.121	0.100
Apical ROI	k_{21}^2	0.765	0.740	0.769	0.765	0.010	0.742	0.765
	k_{12}^2	0.150	0.141	0.150	0.150	0.002	0.142	0.150
	f_v^2	0.150	0.162	0.133	0.150	0.017	0.165	0.150
Lateral ROI	k_{21}^3	0.960	0.771	1.124	0.960	0.043	0.754	0.960
	k_{12}^3	0.600	0.460	0.630	0.600	0.021	0.455	0.600
	f_v^3	0.200	0.294	−0.003	0.200	0.029	0.295	0.200
Septal ROI	k_{21}^4	0.960	0.708	0.976	0.960	0.082	0.628	0.960
	k_{12}^4	0.900	0.644	0.937	0.900	0.056	0.585	0.900
	f_v^4	0.200	0.338	0.271	0.200	0.038	0.333	0.200
Background	g	0.200	0.223	0.200	0.200	0.0001	0.224	0.200

Table 2. Results of kinetic parameter estimation from noiseless, inconsistent, parallel-beam projections: (a) simulated values; (b) values from dynamic reconstructions; (c) values from direct estimation of region time–activity curves (Formiconi 1993); (d) values from direct estimation from projections; (e) uncertainties of values from direct estimation from projections for 3 000 000 events using equation (5). Results of kinetic parameter estimation from noiseless, forced consistent, parallel-beam projections: (b') values from dynamic reconstructions; (c') values from direct estimation of region time–activity curves. The units for k_{21}^m and k_{12}^m are min^{-1} .

		a	b	c	d	e	b'	c'
Main myocardium	k_{21}^1	0.540	0.520	0.539	0.540	0.002	0.522	0.540
	k_{12}^1	0.060	0.060	0.060	0.060	0.0004	0.061	0.060
	f_v^1	0.100	0.135	0.116	0.100	0.004	0.113	0.100
Apical ROI	k_{21}^2	0.765	0.715	0.748	0.765	0.022	0.722	0.765
	k_{12}^2	0.150	0.139	0.148	0.150	0.005	0.141	0.150
	f_v^2	0.150	0.182	0.215	0.150	0.039	0.154	0.150
Lateral ROI	k_{21}^3	0.960	0.718	0.965	0.960	0.096	0.710	0.960
	k_{12}^3	0.600	0.437	0.600	0.600	0.045	0.429	0.600
	f_v^3	0.200	0.351	0.199	0.200	0.066	0.317	0.200
Septal ROI	k_{21}^4	0.960	0.607	1.178	0.960	0.176	0.562	0.960
	k_{12}^4	0.900	0.558	0.988	0.900	0.119	0.523	0.900
	f_v^4	0.200	0.362	0.088	0.200	0.083	0.355	0.200
Background	g	0.200	0.199	0.201	0.200	0.0001	0.199	0.200

the average of the continuously varying value that yielded the inconsistent projections. For the conventional analysis the biases changed very little for the main myocardium and for the apical and lateral ROIs, and increased for the septal ROI. The estimates obtained using Formiconi's method were unbiased for the forced consistent projections, as expected.

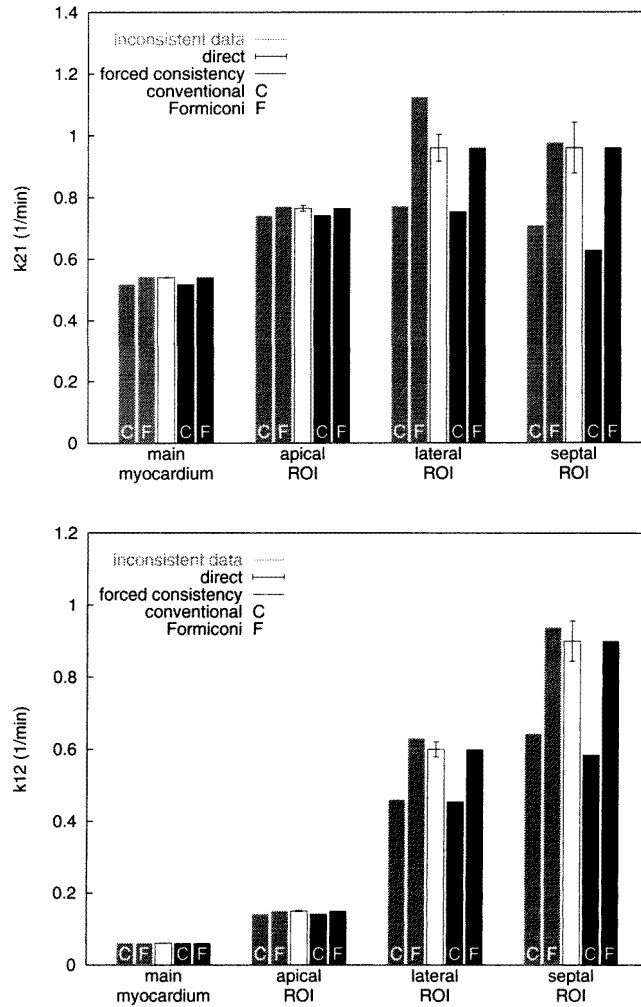


Figure 6. Cone-beam values for k_{21}^m (top) and k_{12}^m (bottom). The grey bars depict the estimates obtained from conventional and Formiconi analyses of noiseless, inconsistent projections. The white bar depicts the unbiased estimate (simulated value) obtained directly from the projections, along with its estimated uncertainty predicted for 10 000 000 events using equation (5). The black bars depict the estimates obtained from conventional and Formiconi analyses of noiseless, forced consistent projections.

Parameter estimates obtained from the noiseless parallel-beam projections had larger biases, compared to those obtained from the cone-beam projections. Biases for the estimates obtained from conventional analysis of inconsistent parallel-beam projections ranged between 4–37% for the uptake parameters and 0–38% for the washout parameters. The biases were again largest for the lateral and septal ROIs. The estimates obtained using Formiconi's method had biases ranging between 0.2–23% for the uptake parameters and 0–10% for the washout parameters. Parameters estimated directly from the noiseless projections were again unbiased and multiple local minima were not encountered regardless of noise levels simulated. Estimated parameter uncertainties (see equation (5)) for 3 000 000

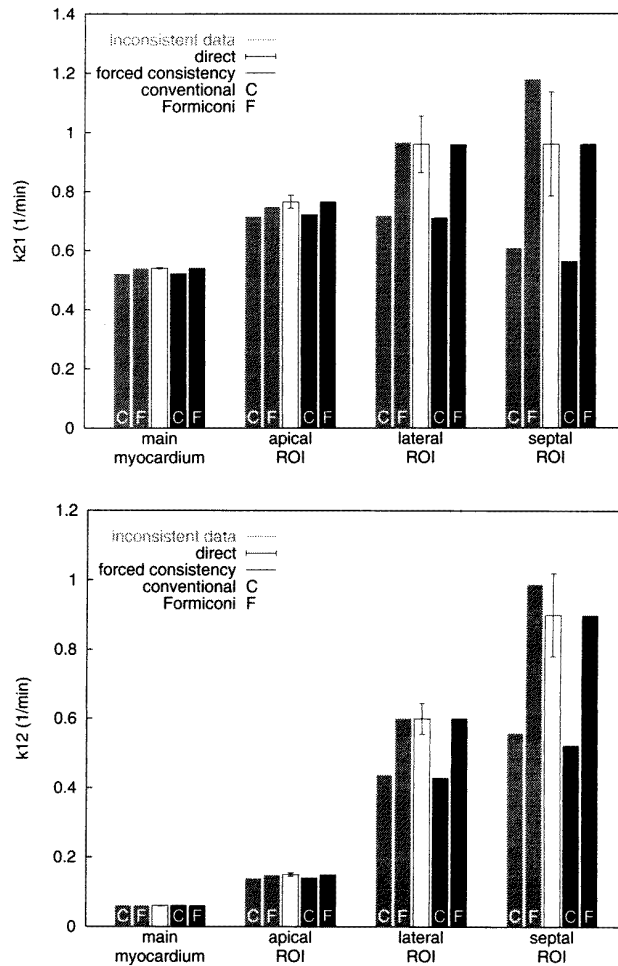


Figure 7. Parallel-beam values for k_{21}^m (top) and k_{12}^m (bottom). The grey bars depict the estimates obtained from conventional and Formiconi analyses of noiseless, inconsistent projections. The white bar depicts the unbiased estimate (simulated value) obtained directly from the projections, along with its estimated uncertainty predicted for 3 000 000 events using equation (5). The black bars depict the estimates obtained from conventional and Formiconi analyses of noiseless, forced consistent projections.

total events ranged between 0.4–18% for the uptake parameters and 0.7–13% for the washout parameters.

For the conventional analysis of noiseless, forced consistent, parallel-beam projections, the biases again changed very little for the main myocardium and for the apical and lateral ROIs, and increased for the septal ROI. The estimates obtained using Formiconi's method were again unbiased.

4. Summary

The combination of gantry motion and the time-varying nature of the radionuclide distribution being imaged results in inconsistent projection data sets. Estimating kinetic

parameters from time–activity curves taken from reconstructed images (Feldkamp *et al* 1984) results in biases. These biases are reduced if the time–activity curves are estimated from the projection data (Formiconi 1993). Estimating the kinetic parameters directly from cone-beam projections removes all bias for noiseless data as expected. Implementation of this strategy requires a spatial and temporal model of the distribution of radionuclide within the SPECT field of view.

Acknowledgments

This work was supported by US Department of Health and Human Services grants R01-HL50663 and P01-HL25840 and by US Department of Energy contract DE-AC03-76SF00098.

References

- Bates D M and Watts D G 1988 *Nonlinear Regression Analysis and Its Applications* (New York: Wiley)
- Carson R E 1986 A maximum likelihood method for region-of-interest evaluation in emission tomography *J. Comput. Assist. Tomogr.* **10** 654–63
- Chiao P C, Rogers W L, Clinthorne N H, Fessler J A and Hero A O 1994a Model-based estimation for dynamic cardiac studies using ECT *IEEE Trans. Med. Imaging* **13** 217–26
- Chiao P C, Rogers W L, Fessler J A, Clinthorne N H and Hero A O 1994b Model-based estimation with boundary side information or boundary regularization *IEEE Trans. Med. Imaging* **13** 227–34
- Defrise M, Townsend D and Geissbuhler A 1990 Implementation of three-dimensional image reconstruction for multi-ring positron tomographs *Phys. Med. Biol.* **35** 1361–72
- Feldkamp L A, Davis L C and Kress J W 1984 Practical cone-beam algorithm *J. Opt. Soc. Am. A* **1** 612–9
- Formiconi A R 1993 Least squares algorithm for region-of-interest evaluation in emission tomography *IEEE Trans. Med. Imaging* **12** 90–100
- Huesman R H 1984 A new fast algorithm for the evaluation of regions of interest and statistical uncertainty in computed tomography *Phys. Med. Biol.* **29** 543–52
- Huesman R H, Reutter B W, Zeng G L and Gullberg G T 1997 Kinetic parameter estimation from SPECT projection measurements *J. Nucl. Med.* **38** (Suppl 5) 222
- Limber M A, Limber M N, Celler A, Barney J S and Borwein J M 1995 Direct reconstruction of functional parameters for dynamic SPECT *IEEE Trans. Nucl. Sci.* **42** 1249–56
- Seber G A F and Wild C J 1989 *Nonlinear Regression* (New York: Wiley)
- Smith A M, Gullberg G T and Christian P E 1996 Experimental verification of ^{99m}Tc-teboroxime kinetic parameters in the myocardium using dynamic SPECT: reproducibility, correlations to flow, and susceptibility to extravascular contamination *J. Nucl. Cardiol.* **3** 130–42
- Smith A M, Gullberg G T, Christian P E and Datz F L 1994 Kinetic modelling of teboroxime using dynamic SPECT imaging of a canine model *J. Nucl. Med.* **35** 984–95
- Zeng G L, Gullberg G T and Huesman R H 1995 Using linear time-invariant system theory to estimate kinetic parameters directly from projection measurements *IEEE Trans. Nucl. Sci.* **42** 2339–46